Enhancement of Resonance by the Use of Multiple Tunnel Barriers in Bilayer Graphene-Based Interlayer Tunnel Field Effect Transistors

Nitin Prasad
Microelectronics Research Center and Dept. of Electrical and Computer Engg. University of Texas at Austin
Austin, TX, USA
nitinprasad@utexas.edu

Sanjay K. Banerjee
Microelectronics Research Center and Dept. of Electrical and Computer Engg. University of Texas at Austin
Austin, TX, USA
banerjee@ece.utexas.edu

Leonard F. Register
Microelectronics Research Center and Dept. of Electrical and Computer Engg. University of Texas at Austin
Austin, TX, USA
register@mer.utexas.edu

***Abstract*—Interlayer tunnel field effect transistors (ITFETs) make use of resonant tunneling between two layers of two-dimensional semiconductors to create a negative differential resistance. A narrow resonance allows for lowering the operating voltages in potential circuit applications. The use of multiple tunnel barriers is investigated as a means to obtain a narrow resonance, as the device dimensions are scaled down. For specificity, we analyze a bilayer graphene-based ITFET system.**

***Keywords*—resonant tunneling; negative differential resistance; transfer Hamiltonian; tunneling transistor.**

I. Introduction

Interlayer tunnel field effect transistors (ITFETs) exploit resonant tunneling between two layers of two-dimensional (2D) van der Waals' semiconductors to obtain a negative differential resistance (NDR) [1]–[7]. NDR has potential applications in digital and analog circuits [8]–[12], and at potentially lower voltages than traditional CMOS technology. To date, ITFET operation has been experimentally demonstrated with graphene [1], [2], bilayer graphene [3], [5] and several layer graphene [4] as the 2D semiconductor. In particular, recent reports have demonstrated high interlayer current densities and a strong resonance with bilayer graphene (BLG)-based ITFETs [5].

A narrow resonance is desirable for reduced operating voltages. With reduction in device dimensions, however, Heisenberg uncertainty due to short channel lengths—the region of overlap between layers through which tunneling occurs—can contribute significantly to resonant broadening [13], [14]. The short-channel-associated broadening is higher for materials with a low-effective mass, such as BLG. In a previous work, we proposed the use of multiple (m) stacked layers of 2D semiconductor and insulator (barriers) to obtain a narrower resonance, referring to the structure as a multi-barrier ITFET (mITFET). The analysis in [14] was done using a fully ballistic approach in which the carriers coherently tunnel across the tunnel barrier stack. In this paper, we describe the transport across the mITFET by allowing the carriers to scatter and thermalize after they tunnel across each tunnel barrier. We use a perturbative approach by describing the tunneling processes through a transfer Hamiltonian. For specificity, we consider BLG, a material with a low electron effective mass of 0.05 m_e, as the 2D material. We show that mITFETs offer conceptually viable way to reduce short-channel broadening, even after including thermal resonant broadening of tunneling between the 2D layers.

This work was supported by the Semiconductor Research Corporation's Nanoelectronics Research Initiative (SRC-NRI) via the South West Academy of Nanoelectronics (SWAN). Supercomputing resources were provided by the Texas Advanced Computing Center (TACC).

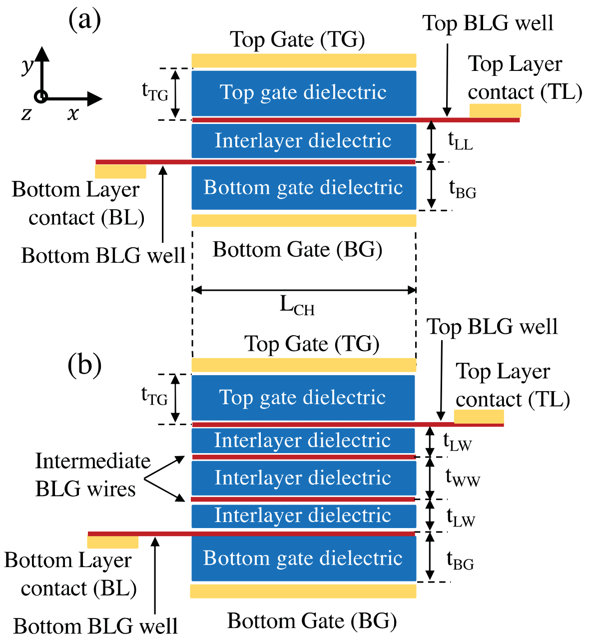

Fig. 1. Cross-section of (a) a single-barrier ITFET with two 2D quantum wells, and (b) a triple barrier mITFET with two 2D quantum wells and two 2D quantum wires.

II. Model Description

A schematic cross-section of an ITFET with a single tunnel barrier is shown in Fig. 1(a). The top (TL) and the bottom (BL) bilayer graphene layers (henceforth referred to as simply *bilayers*) are separated by a thin interlayer dielectric such as hexagonal boron nitride (hBN) or a transition metal dicalcogenide (TMD). The electrostatics within the bilayers can be controlled by the use of top gate (TG) and bottom gate (BG)

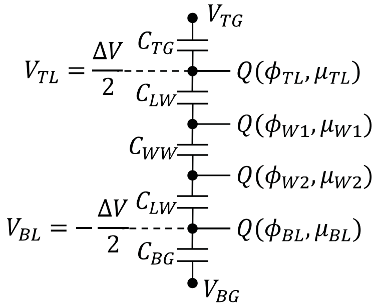

Fig. 2. Capacitive coupling model to estimate the electrostatic potentials of the 2D layers. The additional charges, Q, take into account the quantum capacitance associated with the finite density of states within the bilayers.

as well as the TL and BL contacts. A schematic cross-section of a mITFET with three interlayer tunnel barriers is shown in Fig. 1(b). The A mITFET with n ($n > 0$) barriers has two quantum wells – one top (TL) and one bottom (BL) – that form the leads, and $n - 1$ intermediate quantum wires running normal (along the *y* direction) to the nominal transport direction.

Under the weak coupling limit, the electrostatic (ϕ) and the chemical (μ) potentials are modeled as constant along the nominal transport direction (*x*). For simplicity, the electronic bands are assumed to have a parabolic dispersion near the K-point with electron/hole effective masses of 0.05. We consider two conduction and two valence bands in all calculations. For a given set of gate biases, the band-alignments and the electrostatic potentials are computed using a self-consistent capacitive model (Fig. 2). The additional charges, Q, indicated in Fig. 2 take into account the charging quantum capacitance associated with the finite density of states within the bilayers.

The single particle current between any two layers is computed using a perturbative Hamiltonian approach. The single particle coherent tunneling current flowing from Bilayer *a* to Bilayer *b* is given by

$$I_{\mathrm{ab}} = -e\int_{-\infty}^{\infty} T_{a,b}(E)\big(f(E-\mu_a) - f(E-\mu_b)\big)dE \qquad (1)$$

where $f(E)$ is the Fermi distribution function and $T_{a,b}(E)$ is the vertical transmission rate of an electron from layer a to layer b at an energy E , and is given by

$$T_{a,b}(E) = \frac{2\pi}{\hbar}\sum_{\mathbf{k}_a,\mathbf{k}_\mathrm{b},s_a,s_b}\left|\tau_{\mathbf{k}_a,\mathbf{k}_b,s_a,s_\mathrm{b}}\right|^2 \mathrm{A}(\mathbf{k}_a,\mathrm{s}_a,E)\mathrm{A}(\mathbf{k}_b,\mathrm{s}_b,E) \qquad (2)$$

Here, A is the spectral density function of the energy states which is taken to be Lorentzian in form, i.e.,

$$\mathrm{A}(\mathbf{k},\mathrm{s},E) = \frac{1}{\pi}\frac{\Gamma}{(E-\epsilon(\mathbf{k},\mathrm{s}))^2 + \Gamma^2}\ , \qquad (3)$$

where Γ represents the energy broadening of the quasi-particle states, s is the sub-band index and $\hbar\mathbf{k} = \hbar(k_\mathrm{x}\hat{\mathbf{x}} + k_\mathrm{y}\hat{\mathbf{y}})$ is the crystal momentum. We note that Γ also may contain contributions from the spatial variation in the electrostatic potential difference between layers due to disorder.

The electron wavefunctions in the bilayers are assumed have plane wave solutions with appropriate boundary conditions. The tunneling matrix elements $\tau_{\mathbf{k}_a,\mathbf{k}_b,s_a,s_b}$ between any two given layers n and m is calculated by evaluating

$$\tau_{\mathbf{k}_a,\mathbf{k}_b,s_a,s_b} = \langle\psi_\mathrm{a}|H_{Ta,b}|\psi_\mathrm{b}\rangle = \tau_{a,b}\langle\psi_a|\psi_b\rangle, \qquad (4)$$

where the transfer Hamiltonian $H_{\mathrm{T}_{a,b}}$ between layers a and b to be a constant scalar coupling parameter $\tau_{a,b}$. Upon evaluating (4), we obtain,

$$\left|\tau_{\mathbf{k}_a,\mathbf{k}_b,s_a,s_b}\right|^2 = 4\tau_{a,b}^2\delta(k_{y,a} - k_{y,b}) \times \left|\frac{\sin(L_\mathrm{ch}k_{x,a}) - \sin(L_\mathrm{ch}k_{x,b})}{k_\mathrm{xa} - k_\mathrm{xb}} - \frac{\sin(L_\mathrm{ch}k_{x,a}) + \sin(L_\mathrm{ch}k_{x,b})}{k_{x,a} + k_{x,b}}\right|^2. \qquad (5)$$

τ_ab is assumed to follow a power law scaling with change in the tunnel dielectric thickness[15] as

$$\tau_{a,b} = \tau_{1\mathrm{nm}} \times 10^{-(t_\mathrm{a,b} - 1\ \mathrm{nm})/t_0}\ , \qquad (6)$$

where $\tau_{1\ \mathrm{nm}}$ is the interlayer coupling between the layers at a tunnel barrier thickness of 1 nm, $t_{a,b}$ is the tunnel barrier thickness between layers *a* and *b*, and t_0 is the characteristic decay length for the tunneling probability, taken simply as 1 nm here.

In case of bilayer graphene-based ITFETs, momentum-conserving tunneling also is possible from valence to conduction bands (and vice versa) [5]. This is included in the model by ensuring that the tunnel matrix elements in (5) have no explicit dependence on the sub-band indices s_a and s_b.

If Bilayer *a*, Bilayer *b*, or both, form intermediate wires, the crystal momenta of each subband in the corresponding bilayer are discretized along x and are given by

$$k_{x,a} = \frac{n\pi}{L_\mathrm{ch}}\text{, and/or } k_{x,b} = \frac{m\pi}{L_\mathrm{ch}},\ (n,m) \in \{1,2,3,\ldots\} \qquad (7)$$

and the corresponding summation over the momenta in (2) is restricted to these values. However, if Bilayer *a*, Bilayer *b* or both form the top or the bottom bilayers semi-infinite lead contacts, the momentum states are assumed to be continuous. The summation (or integral for lead bilayers) in (2) is performed over a range of momentum states around the K-point in the Brillouin zone.

The top and the bottom layer chemical potentials are controlled by the respective applied lead voltages and can be tuned independently. However, the chemical potentials of the intermediate wires are controlled by the electric fields and the charge in those wires resulting from current flow across the tunnel barrier stack. Therefore, the chemical potential in the intermediate wires is calculated by self-consistently solving the Poisson's equation and by balancing the net in-current and out-current in each layer. Fig. 3(a) shows a convergence algorithm to self-consistently estimate the electric and chemical potentials in the intermediate wires.

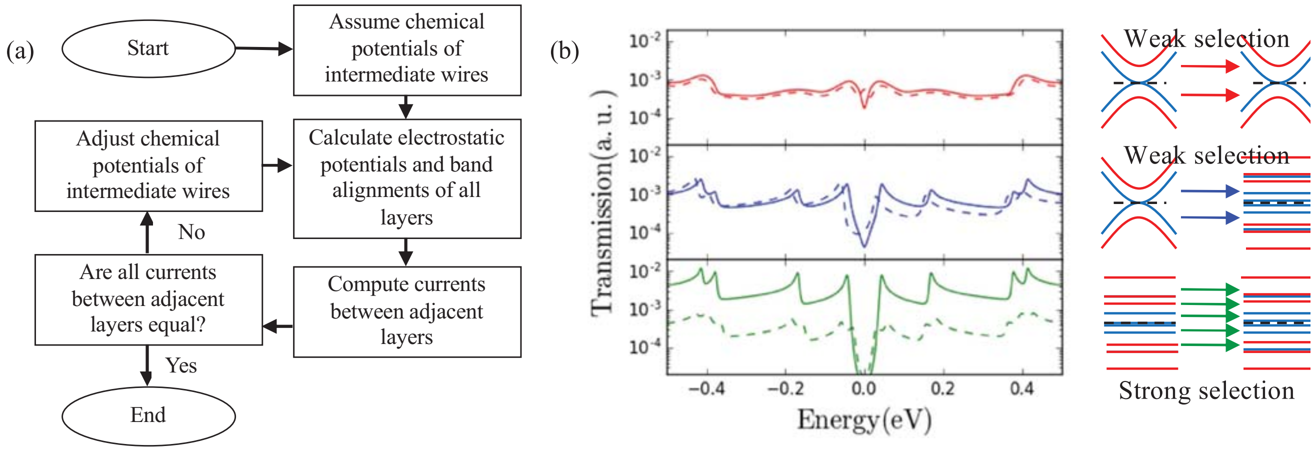

Fig. 3. (a) Convergence algorithm for self-consistent calculation of electrostatic and chemical potentials. (b) Transmission probability at $k_y = 0$ as a function of energy of injection for (top) well-to-well injection (middle) well-to-wire injection, and (bottom) wire-to-wire injection. Solid lines corresponds to transmission probability when the bands are aligned, and dashed line corresponds to that when the bands are out of alignment by 30 meV. All plots are for a device with channel length 15 nm, energy broadening of 5 meV an interlayer coupling of 0.1 meV.

III. Results and Discussion

For specificity, the channel lengths of mITFET are presumed to be 15 nm. The nominal dielectric thickness and constant are presumed to be 1 nm and 3, respectively. All calculations are performed for 300 K, and the energy eigenstates are assumed to be a Lorentzian with a broadening (Γ) of 5 meV [5]. Interlayer coupling between the layers is presumed to be 0.1 meV at a tunnel barrier thickness of 1 nm.

Fig. 3(b) shows the transmission probability between two bilayers, across a single tunnel barrier, as a function of energy for a zero k_y. Note that the transmission functions are peaked around the discretized energy states of the quantum wires when tunneling in or out of the states of the wires. Furthermore, as the bands are taken out of alignment, the greatest suppression in transmission occurs in wire-to-wire transmission. The transmission between the eigenstates of the quantum wires is very selective because, in contrast to tunneling from/to the lead quantum wells, it is not subject to short-channel Heisenberg uncertainty. The increase in the transmission around energies of ±0.37 eV is because of the contributions to the tunneling from the second conduction and valence band around the K-point.

For a fixed set of gate biases, in general, the band structures of all the 2D layers do not align at the same inter-lead voltage (ΔV). This misalignment can result in a significant drop in the peak current as ΔV is varied. To maintain appreciable interlayer currents, we now take advantage of the weak selection between the well-wire states, which becomes weaker with the reduction in the channel length. That is, we now take advantage of Heisenberg uncertainty for tunneling from/to the lead quantum wells. If the thickness of the dielectric barrier between the quantum wires (t_{WW}) is greater than that between the lead wells and the wires (t_{LW}), the applied lead voltages will have a better electrostatic control over the quantum wires, making it easier to pull them in and out of resonance. Furthermore, increase in t_{WW} also reduces the band misalignment between the well and wire states with the applied inter-lead biases. By appropriately sizing the interlayer dielectric thicknesses, one could design a triple-barrier mITFET to show resonant behavior around the voltages when the wire states are aligned, even as the well-to-wire states are misaligned. In Fig. 4(a) and 4(b), we increase the t_{WW} and track the resonant characteristics. We note from Fig. 4(a) that increasing the barrier thickness results in a reduced interlayer drive current because of reduced interlayer coupling, following (6). However, an increase in t_{WW} also results in the sharpening of the resonance because of better electrostatic control, as seen in the differential conductance at zero gate biases in Fig. 4 (d). Therefore, with a uniform dielectric as assumed for these calculations, one has to trade off the drive current with resonant width, while choosing appropriate dielectric thicknesses in the tunnel barrier stack. Henceforth, we assume the intermediate case of t_{WW} to be 1.5 nm for a triple-barrier mITFET. However, in principle, one could vary the tunnel dielectric materials between the bilayers to appropriately adjust the electrostatics and tunneling strength to optimize lead voltage control and tunneling strength somewhat independently.

The current characteristics of a triple-barrier mITFET shows multiple peaks as the interlead voltage is varied. To understand the origin of multiple resonant peaks, we plot various band alignments across the bilayers corresponding to different interlead voltages labelled in Fig. 4 (a). Note that the energy of states in the quantum well leads are shown to be continuously varying with momentum, while the energy states in the wires are discretized. At $\Delta V = V_2$ all the eigenstates of the two wells align. Although there is a small misalignment between the states of the wells and wires, resonant current flows because of the weak selection rules between the wells and wires. At $\Delta V = V_1, V_3$, secondary current resonances are caused by transmission between the first conduction sub-band in one wire to that of the valence band in the other wire. These latter resonances are lower broader because the peak represents only the onset of quantum wire subband overlap, with the subband energy vs. momentum dispersions curving in opposite directions with respect to energy. As channel lengths decreases, the energy separation between the quantized states of the wires increases, thereby

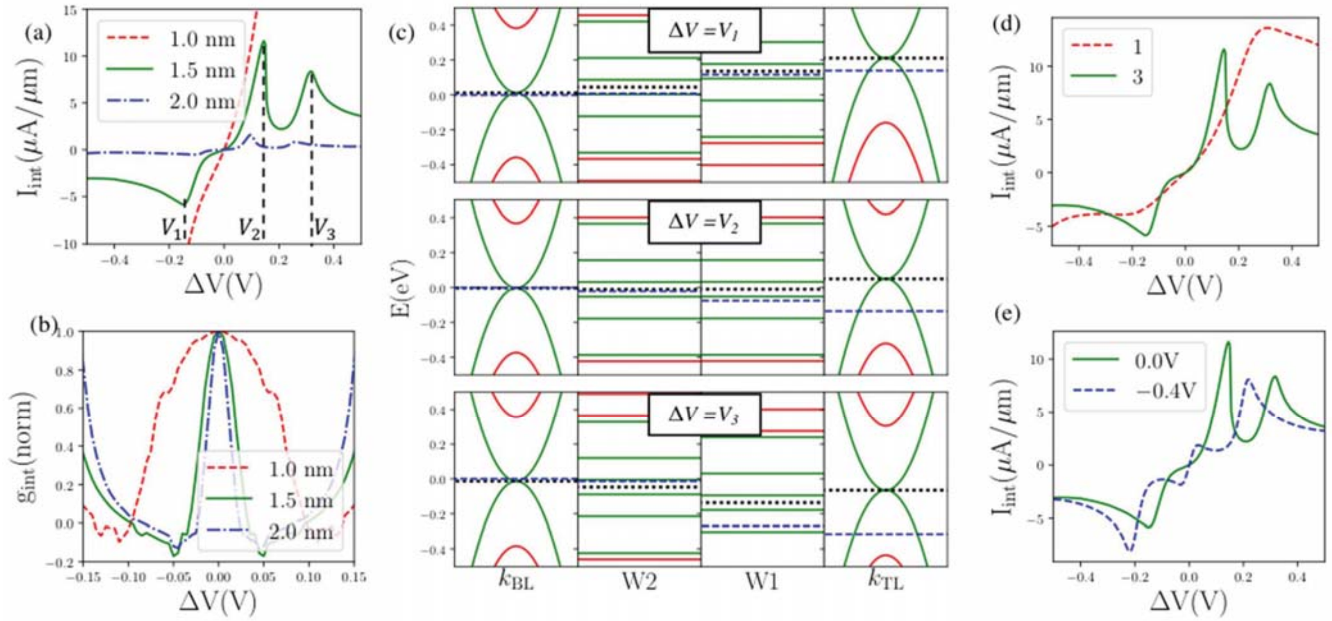

Fig. 4. (a) I-V characteristics of a triple barrier mITFET at $V_{TG} = -0.4V$ with various t_{WW} shown in the legend. (b) Normalized differential conductance of a triple barrier mITFET at $V_{TG} = 0V$. Note the reduction in interlayer current in (a) and resonance width in (b). (c) Band alignments illustrating various resonance conditions at three voltages labeled in (a), where: the solid lines represent the continuous and discrete band structures in the direction of transport of the wells and wires, respectively; the dotted lines represent the conduction/valence band edge; and the dashed lines the, the Fermi levels. I-V characteristics of a triple (3) barrier mITFET (d) compared to a single (1) barrier ITFET, at $V_{\mathrm{TG}} = -0.4\ V$ (e) at different V_{TG} shown in the legend. ΔV is the inter-lead voltage. The interlayer coupling of the triple barrier ITFET is approximately 3 times that of the single barrier mITFET. The bottom gate is grounded in all calculations.

causing the secondary resonances to be pushed further away from the primary resonance.

Fig. 4(d) compares the current characteristics as a function of the inter-lead voltage of a triple barrier mITFET to that of a single barrier ITFET. To get comparable drive currents, the nominal coupling value between bilayers separated by a fixed thickness of the triple barrier mITFET is approximately three times that of a single barrier ITFET. Fig. 4(e) illustrates the interlead resonance voltage by applied gate bias, to the top gate only in this case.

IV. Conclusion

We show that the short channel associated resonance broadening potentially could be reduced with the use of additional tunnel barriers to create a mITFET variant of ITFETs. By carefully engineering the tunnel barrier stack dielectrics, one can trade off between the magnitude of the tunneling current and the resonance width. Alternatively, it also may be possible to alternated dialectics to further optimize current and resonance width. The reduction in the resonance broadening that may be possible with mITFETs would lead to reduced operating voltages and power consumption in circuits.

References

[1] L. Britnell *et al.*, "Resonant tunnelling and negative differential conductance in graphene transistors," *Nature Communications*, vol. 4, p. ncomms2817, Apr. 2013.

[2] A. Mishchenko *et al.*, "Twist-controlled resonant tunnelling in graphene/boron nitride/graphene heterostructures," *Nature Nanotechnology*, vol. 9, no. 10, pp. 808–813, Oct. 2014.

[3] B. Fallahazad *et al.*, "Gate-Tunable Resonant Tunneling in Double Bilayer Graphene Heterostructures," *Nano Letters*, vol. 15, no. 1, pp. 428–433, 2015.

[4] S. Kang *et al.*, "Effects of Electrode Layer Band Structure on the Performance of Multilayer Graphene–hBN–Graphene Interlayer Tunnel Field Effect Transistors," *Nano Lett.*, vol. 16, no. 8, pp. 4975–4981, Aug. 2016.

[5] G. W. Burg *et al.*, "Coherent Interlayer Tunneling and Negative Differential Resistance with High Current Density in Double Bilayer Graphene–WSe2 Heterostructures," *Nano Lett.*, vol. 17, no. 6, pp. 3919–3925, Jun. 2017.

[6] R. M. Feenstra, D. Jena, and G. Gu, "Single-particle tunneling in doped graphene-insulator-graphene junctions," *Journal of Applied Physics*, vol. 111, no. 4, p. 043711, Feb. 2012.

[7] S. C. de la Barrera and R. M. Feenstra, "Theory of resonant tunneling in bilayer-graphene/hexagonal-boron-nitride heterostructures," *Applied Physics Letters*, vol. 106, no. 9, p. 093115, Mar. 2015.

[8] S. Mohan, P. Mazumder, G. I. Haddad, R. K. Mains, and J. P. Sun, "Logic design based on negative differential resistance characteristics of quantum electronic devices," *IEE Proceedings G (Circuits, Devices and Systems)*, vol. 140, no. 6, pp. 383–391, Dec. 1993.

[9] J. A. Simmons, M. A. Blount, J. S. Moon, W. E. Baca, J. L. Reno, and M. J. Hafich, "Unipolar complementary bistable memories using gate-controlled negative differential resistance in a 2D-2D quantum tunneling transistor," in *International Electron Devices Meeting. IEDM Technical Digest*, 1997, pp. 755–758.

[10] J. I. Bergman *et al.*, "RTD/CMOS nanoelectronic circuits: thin-film InP-based resonant tunneling diodes integrated with CMOS circuits," *IEEE Electron Device Letters*, vol. 20, no. 3, pp. 119–122, Mar. 1999.

[11] Y. Ando, "Negative differential resistance amplifier," US5920231A, 06-Jul-1999.

[12] D. Reddy, L. F. Register, E. Tutuc, and S. K. Banerjee, "Bilayer Pseudospin Field-Effect Transistor: Applications to Boolean Logic," *IEEE Transactions on Electron Devices*, vol. 57, no. 4, pp. 755–764, Apr. 2010.
[13] X. Wu, X. Mou, L. F. Register, and S. K. Banerjee, "Full-band simulations of single-particle resonant tunneling in transition metal dichalcogenide-based interlayer tunneling field-effect transistors," in *2016 Simulation of Semiconductor Processes and Devices (SISPAD)*, 2016, pp. 89–92.
[14] N. Prasad, X. Mou, L. F. Register, and S. K. Banerjee, "Multi-barrier inter-layer tunnel field-effect transistor," in *2016 IEEE International Electron Devices Meeting (IEDM)*, 2016, pp. 30.4.1-30.4.4.
[15] S. Kang *et al.*, "Interlayer tunnel field-effect transistor (ITFET): physics, fabrication and applications," *J. Phys. D: Appl. Phys.*, vol. 50, no. 38, p. 383002, 2017.